Electron Transport and Hot Phonons in Carbon Nanotubes

Michele Lazzeri,[1] S. Piscanec,[2] Francesco Mauri,[1] A. C. Ferrari,[2] and J. Robertson[2]

[1]*Institut de Minéralogie et de Physique des Milieux Condensés, 4 Place Jussieu, 75252, Paris cedex 05, France*
[2]*Engineering Department, Cambridge University, Trumpington Street, Cambridge CB2 1PZ, United Kingdom*

We demonstrate the key role of phonon occupation in limiting the high-field ballistic transport in metallic carbon nanotubes. In particular, we provide a simple analytic formula for the electron transport scattering length, which we validate by accurate first principles calculations on $(6, 6)$ and $(11, 11)$ nanotubes. The comparison of our results with the scattering lengths fitted from experimental I-V curves indicates the presence of a nonequilibrium optical phonon heating induced by electron transport. We predict an effective temperature for optical phonons of thousands Kelvin.

PACS numbers: 73.63.Fg, 63.20.Kr, 73.22.−f

Single wall carbon nanotubes (SWNTs) have unique properties that make them strong candidates for future electronic devices. They can act as one-dimensional quantum wires with ballistic electron transport [1–3]. Because of the strong C-C bond, they can carry the highest current density of any material before they break. This makes them the best candidates as interconnects in integrated circuits and for high performance field effect transistors. It is thus essential to understand what ultimately limits the high current performance of nanotube devices. High-field transport measurements have shown that electron-phonon coupling limits the ballistic behavior [4–6]. At high bias (≥ 0.2 V) electrons scatter with optical phonons, while at low bias (< 0.2 V) they scatter with acoustic phonons. Ballistic transport is possible up to few hundreds nanometers in low bias, but the electron mean free path significantly drops at high bias [4–6]. By constructing devices smaller than the high-bias scattering length, a boost in performance is achieved [7,8].

The Boltzmann theory is used in Refs. [4–6] to fit the scattering length (l_{op}) from the measured I-V curves. It is striking that the analysis of several SWNTs, with 1–3 nm diameters, gives a similar $l_{\mathrm{op}} \sim 10$–15 nm for optical-phonon backscattering [4–6]. Alternatively, the scattering lengths could be derived knowing (i) the electron-phonon coupling (EPC) and (ii) the phonon occupation during transport. Thus, if the EPC is independently known, the phonon occupation can be derived from the experimentally fitted scattering length. A reliable determination of the EPC is essential to apply this procedure.

Several attempts to determine the EPC using tight binding (TB) have been reported [4,6,9–13]. The predicted EPCs are not reliable since they strongly depend on the TB parametrization used. For example, for the graphene unit cell and the E_{2g} phonon, the maximum of the EPC square at $\boldsymbol{\Gamma}$ $|D_{\boldsymbol{\Gamma}}^{\max}|^2$ has been calculated to be 17, 42, 35/58, and 164 (eV/Å)^2 in Refs. [9], [12,14], [10,14], and [6], respectively. These numbers give an order of magnitude spread in the calculated scattering length, this being proportional to $|D_{\boldsymbol{\Gamma}}^{\max}|^2$. On the other hand, the

optical-phonon EPCs were never directly measured. But we recently showed that graphite EPCs can be directly determined from the experimental phonon dispersions or from the Raman D-peak dispersion [15]. The measured EPCs are in excellent agreement with accurate density functional theory (DFT) calculations [15]. This confirms the reliability of DFT for determining the EPCs in graphitic materials, such as SWNTs.

In this Letter, we demonstrate the key role of phonon occupation in limiting the high-field transport in nanotubes. To do so, we use DFT to compute with high accuracy the optical-phonon EPCs in $(6, 6)$ and $(11, 11)$ SWNTs. We demonstrate that curvature does not affect the EPCs in SWNTs with diameters $\gtrsim 0.8$ nm, such as those used in transport measurements [4–8]. Then we prove that the EPCs for SWNTs of arbitrary chirality can be derived from those of graphite, by using a simple analytic formula. We use our computed and measured [15] EPCs to obtain the electron mean free path for optical phonon scattering in high-field quasiballistic transport. We obtain the phonon occupation by comparing our scattering length with the l_{op} fitted in transport measurements.

SWNTs are identified by the chiral indices (n, m), giving the chiral vector $\mathbf{C_h} = n\mathbf{a_1} + m\mathbf{a_2}$, with $\mathbf{a_1}$ and $\mathbf{a_2}$ the graphene lattice vectors [16]. A SWNT is obtained by folding graphene so that the two atoms connected by $\mathbf{C_h}$ coincide. In real space, a SWNT is periodic along its axis according to the translational vector $\mathbf{T}$ [16]. For diameters $\gtrsim 0.8$ nm the electron states are very well described by the folded graphene bands [17]. Thus, we can safely use zone folding to describe the states relevant to charge transport. The SWNT electron states correspond to the graphene states having periodicity $\mathbf{C_h}$, i.e., such that $\mathbf{k} \cdot \mathbf{C_h} = 2\pi o$, o being an integer. The SWNT electron states are labeled by two-dimensional momentum vectors $\mathbf{k}$, which cut with a series of parallel lines the graphene Brillouin zone (BZ) [16].

The SWNT optical phonon frequencies are modified by the quantum confinement of electron states along the circumference [15,18,19]. For diameters $\gtrsim 0.8$ nm, the de-

viation of the SWNT phonon frequencies from folded graphene is $\leq 5\%$ [19]. Such deviation has a negligible impact on scattering lengths. Thus, we use zone folding to describe SWNT phonon frequencies and eigenmodes, and we label the phonons by a two-dimensional momentum vector $\mathbf{q}$ in the graphene BZ. The SWNT electron and phonon states are normalized in the one-dimensional SWNT unit cell, with period $\mathbf{T}$.

The decay time for an electron state $\mathbf{k}$, band i, and energy $\epsilon_{\mathbf{k}i}$ into the electron band j and energy $\epsilon_{(\mathbf{k}+\mathbf{q})j}$, due to scattering with $\mathbf{q}$ or $-\mathbf{q}$ phonons in branch η, and with energy $\hbar\omega_{\mathbf{q}\eta}$, is given by the Fermi golden rule [20]:

$$\frac{1}{\tau} = \frac{2\pi}{\hbar N}\sum_{\mathbf{q}\eta}|g_{(\mathbf{k}+\mathbf{q})j,\mathbf{k}i}|^2\{\delta[\epsilon_{\mathbf{k}i} - \epsilon_{(\mathbf{k}+\mathbf{q})j} + \hbar\omega_{\mathbf{q}\eta}]n_{\mathbf{q}\eta}$$
$$+ \delta[\epsilon_{\mathbf{k}i} - \epsilon_{(\mathbf{k}+\mathbf{q})j} - \hbar\omega_{\mathbf{q}\eta}](n_{-\mathbf{q}\eta} + 1)\}, \quad (1)$$

where N is the number of q points, the two Dirac δ distributions describe the processes of phonon absorption and emission, and $n_{\mathbf{q}\eta}$ is the phonon occupation number. For thermal equilibrium, $n_{\mathbf{q}\eta}$ is the Bose-Einstein occupation factor $n_{\mathbf{q}\eta} = [\exp(\hbar\omega_{\mathbf{q}\eta}/k_BT) - 1]^{-1}$. Within DFT, the EPC is defined as $g_{(\mathbf{k}+\mathbf{q})j,\mathbf{k}i} = D_{(\mathbf{k}+\mathbf{q})j,\mathbf{k}i}\sqrt{\hbar/(2M\omega_{\mathbf{q}\eta})}$, where M is the atomic mass,

$$D_{(\mathbf{k}+\mathbf{q})j,\mathbf{k}i} = \langle\mathbf{k} + \mathbf{q}, j|\Delta V_{\mathbf{q}\eta}|\mathbf{k}, i\rangle, \quad (2)$$

$|\mathbf{k}, i\rangle$ is the electron state, and $\Delta V_{\mathbf{q}\eta}$ is the Kohn-Sham potential derivative with respect to phonon displacement.

For optical phonons, the phonon dispersion is much smaller than the electron band dispersion. Thus, considering only phonon emission, i.e., only the second δ, Eq. (1) becomes

$$\frac{1}{\tau} = \sum_{\eta}\frac{\pi}{M\omega_{\mathbf{q}\eta}}|D_{(\mathbf{k}+\mathbf{q})j,\mathbf{k}i}|^2\rho[\epsilon_{(\mathbf{k}+\mathbf{q})j}](n_{-\mathbf{q}\eta} + 1), \quad (3)$$

where $\rho[\epsilon_{(\mathbf{k}+\mathbf{q})j}]$ is the electron density of states for band j, and $\mathbf{q}$ is fixed by $\epsilon_{(\mathbf{k}+\mathbf{q})j} = \epsilon_{\mathbf{k}i} - \hbar\omega_{\mathbf{q}\eta}$.

For graphene, the electronic gap is zero for the π bands at the two equivalent BZ points $\mathbf{K}$ and $\mathbf{K}' = 2\mathbf{K}$. Metallic SWNTs have electron states corresponding to the graphene $\mathbf{K}$ and $2\mathbf{K}$ points. For bias smaller than 1.0 V, the mobile electrons belong to π bands near the Fermi energy ϵ_F. Both the initial and final states, $\mathbf{k}$ and $\mathbf{k} + \mathbf{q}$, are close to $\mathbf{K}$ or to $2\mathbf{K}$. The π bands can be considered linearly dispersive, crossing at ϵ_F with slopes β and $-\beta$, with $\beta = 5.52$ Å eV, and density of states $\rho[\epsilon_{(\mathbf{k}+\mathbf{q})j}] = T/(2\pi\beta)$. Phonons connect electron states near ϵ_F only for $\mathbf{q} \simeq \boldsymbol{\Gamma}$ or for $\mathbf{q} \simeq \mathbf{K}$; thus, in Eq. (3), $\omega_{\mathbf{q}\eta}$ can be approximated by $\omega_{\boldsymbol{\Gamma}\eta}$ or by $\omega_{\mathbf{K}\eta}$. After the scattering, the electron can either maintain its propagation direction (forward scattering) or reverse it (backscattering). We thus have four possible scattering processes; see Fig. 1. We label the corresponding decay times $\tau_{\boldsymbol{\Gamma}}^{bs}$, $\tau_{\mathbf{K}}^{bs}$, $\tau_{\boldsymbol{\Gamma}}^{fs}$, and $\tau_{\mathbf{K}}^{fs}$. The total decay time is given by $1/\tau = 1/\tau_{\boldsymbol{\Gamma}}^{bs} + 1/\tau_{\mathbf{K}}^{bs} + 1/\tau_{\boldsymbol{\Gamma}}^{fs} + 1/\tau_{\mathbf{K}}^{fs}$. To model the transport with Boltzmann [4,5], one needs to know the
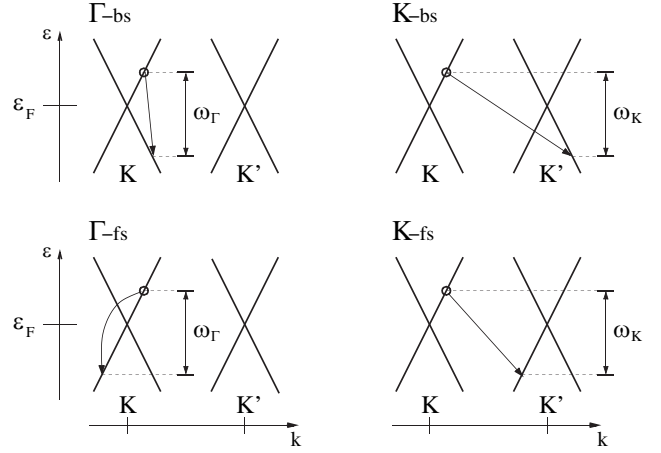

FIG. 1. Conduction band electrons in a metallic SWNT. First order decay induced by the emission of a phonon with frequency $\omega_{\mathbf{q}}$. An electron state can be scattered into the same band by forward scattering (fs) or into another band by backscattering (bs). The resulting four possible processes are labeled by the phonon vector ($\boldsymbol{\Gamma}$ or $\mathbf{K}$) and by the type of scattering (fs or bs). ϵ_F is the Fermi energy.

decay times for each individual process. Possible scattering into higher energy bands is neglected. This assumption is valid for electron energies lower than $2\beta/d$, d being the tube diameter. Note that the electron-phonon scattering processes involved in electron transport are entirely analogous to those involved in Raman spectroscopy [15,21,22].

We now compute the SWNT EPCs by folding the corresponding graphene EPCs. We then demonstrate the validity of this approach, which, so far, has never been proven. The EPC (D) for a SWNT of arbitrary chirality can be obtained from the graphene EPC ($\tilde{D}$), using:

$$S|D_{(\mathbf{k}+\mathbf{q})i,\mathbf{k}j}|^2 = \tilde{S}|\tilde{D}_{(\mathbf{k}+\mathbf{q})i,\mathbf{k}j}|^2, \quad (4)$$

where $\tilde{S} = a_0^2\sqrt{3}/2$ is the graphene unit-cell surface, $a_0 = 2.46$ Å is the graphene lattice spacing, and $S = |\mathbf{C_h} \times \mathbf{T}|$ is the nanotube unit-cell surface [16]. Equation (4) comes from Eq. (2), using the appropriate normalization of phonon and electron states. Combining all the previous results, for metallic SWNTs, Eq. (3) becomes

$$\frac{1}{\tau} = \frac{1}{d}\sum_{\eta}\frac{\sqrt{3}a_0^2|\tilde{D}_{(\mathbf{k}+\mathbf{q})j,\mathbf{k}i}|^2}{4\pi M\omega_{\mathbf{q}\eta}\beta}(n_{-\mathbf{q}\eta} + 1), \quad (5)$$

where $d = C_h/\pi = a_0\sqrt{n^2 + nm + m^2}/\pi$ is the diameter.

For electron states near ϵ_F in graphene, $|\tilde{D}|^2$ is not negligible only for the $\boldsymbol{\Gamma}$ E_{2g} and $\mathbf{K}$ A_1' modes [15]. For optical phonons near $\boldsymbol{\Gamma}$, the doubly degenerate E_{2g} mode splits into two almost longitudinal (LO) and transverse (TO) modes. For small $\mathbf{k}'$, the corresponding EPCs are

$$|\tilde{D}_{(\mathbf{K}+\mathbf{k}'+\mathbf{q})\pi^*,(\mathbf{K}+\mathbf{k}')\pi}^{LO/TO}|^2 = \langle\tilde{D}_{\boldsymbol{\Gamma}}^2\rangle_F[1 \pm \cos(\theta + \theta')],$$
$$|\tilde{D}_{(\mathbf{K}+\mathbf{k}'+\mathbf{q})\pi^*,(\mathbf{K}+\mathbf{k}')\pi^*}^{LO/TO}|^2 = \langle\tilde{D}_{\boldsymbol{\Gamma}}^2\rangle_F[1 \mp \cos(\theta + \theta')], \quad (6)$$

with θ the angle between $\mathbf{k}'$ and $\mathbf{q}$, θ' the angle between $\mathbf{k}' + \mathbf{q}$ and $\mathbf{q}$, and π and π^* are the lower and higher π bands [15]. $+$ or $-$ refer to the LO and the TO modes, respectively. For the $\mathbf{K} - A_1'$ mode, we have

$$|\tilde{D}_{(2\mathbf{K}+\mathbf{k}'+\mathbf{q}')\pi^*,(\mathbf{K}+\mathbf{k}')\pi}|^2 = \langle \tilde{D}_\mathbf{K}^2 \rangle_F (1 + \cos\theta''),$$
$$|\tilde{D}_{(2\mathbf{K}+\mathbf{k}'+\mathbf{q}')\pi^*,(\mathbf{K}+\mathbf{k}')\pi^*}|^2 = \langle \tilde{D}_\mathbf{K}^2 \rangle_F (1 - \cos\theta''), \quad (7)$$

where θ'' is the angle between $\mathbf{k}'$ and $\mathbf{k}' + \mathbf{q}'$ [23]. From our DFT calculations, $\langle \tilde{D}_\Gamma^2 \rangle_F = 45.60$ (eV/Å)^2 and $\langle \tilde{D}_\mathbf{K}^2 \rangle_F = 92.05$ (eV/Å)^2 [14,15]. These values reproduce very accurately the EPCs extracted from the measured graphite phonon dispersion [15].

From Eqs. (6) and (7), we obtain the EPCs for all the scattering processes in Fig. 1. The results are in Table I. Note that, for metallic SWNTs, $\mathbf{k}'$ and $\mathbf{q}$ or $\mathbf{q}'$ are always parallel to the axis, and θ, θ', and θ'' are always equal to 0 or π. Thus, the results of Table I do not depend on chirality.

Using Eq. (5) and Table I, we can easily compute the scattering length l ($l = \tau\beta/\hbar$) for a generic metallic SWNT:

$$l_{\mathbf{q}\eta} = \alpha_{\mathbf{q}\eta} d/(n_{-\mathbf{q}\eta} + 1); \qquad \alpha_{\mathbf{q}\eta} = \frac{4\pi}{\sqrt{3}} \frac{M\omega_{\mathbf{q}\eta}\beta^2}{\hbar a_0^2 |\tilde{D}|^2}. \quad (8)$$

In Refs. [4–6], phonons are assumed thermalized at room temperature ($n_{-\mathbf{q}\eta} \simeq 0$) and the contribution of forward scattering is neglected. Thus, to compare with experiments, we consider only backscattering and define $l_{op} = (1/l_\mathbf{K}^{bs} + 1/l_{\Gamma\,LO}^{bs})^{-1}$. Using the graphene phonon frequencies ($\omega_\Gamma = 196.0$ meV, $\omega_\mathbf{K} = 161.2$ meV) [15], we obtain the results of Table II. In particular, we get a simple scaling between scattering length and diameter:

$$l_{op} = 65d. \quad (9)$$

To validate these results, we perform an explicit calculation of $|D|^2$ on $(6, 6)$ and $(11, 11)$ armchair SWNTs. DFT calculations are done with the gradient corrected functional of Ref. [24]. We use plane waves (40 Ry cutoff) and pseudopotential approaches [25]. Electron states are occupied with an Hermite-Gauss smearing of order 1 and a width of 0.05 Ry [26]. EPC calculations are done using the perturbative method of Ref. [27]. We use an hexagonal supercell with a neighboring tube distance of 5 Å and a grid of 16 k points with a logarithmic distribution around the $\mathbf{K}$ point. In Table II we report the scattering lengths obtained using the $|D|^2$ computed explicitly for the two tubes. Table II shows that the zone-folding results are quite accurate for the 1.5 nm diameter tube, and only a $<20\%$

difference is present for the smaller-diameter tube, due to curvature effects.

Thus, Eq. (8), combined with our *computed and measured* graphite EPCs [15], provides an independent assessment of the scattering lengths for the 1–3 nm diameter SWNTs of Refs. [4–6]. However, the scattering length reported in Refs. [4–6] is ~10–15 nm. This is 1 order of magnitude smaller than what is predicted by Eq. (9). This disagreement cannot be attributed entirely to the experimental uncertainty in measuring the scattering lengths, since three independent experiments on a variety of different tubes obtained very similar results [4–6]. Also, it cannot be ascribed to an error in the DFT EPCs, since our computed EPCs reproduce very well those extracted from the experimental graphite phonon dispersions or from the Raman D-peak dispersion [15]. Thus, we conclude that the hypothesis of thermalized phonon occupation [$n_{-\mathbf{q}\eta} \simeq 0$ in Eq. (8)] does not hold.

A significant phonon occupation n can explain the small value of the measured scattering length l_{op}. This hot phonon generation can occur if, during high-field electron transport, the optical-phonon excitation rate is faster than their thermalization rate. With a high phonon occupation, both phonon emission and absorption processes are equally relevant. We can estimate the scattering lengths by assuming that the phonon occupation n is independent of $\mathbf{q}$ and η and by summing the absorption and emission contributions. The scattering lengths are then obtained by substituting ($n_{-\mathbf{q}\eta} + 1$) with ($2n + 1$) in Eq. (8):

$$l_{op} = 65d/(2n + 1). \quad (10)$$

n in the 2.7–5 range is necessary to reconcile the scattering lengths derived from the computed and measured EPCs and form the fit of the measured I-V curves. This corresponds to an effective temperature for the occupation of optical modes $\gtrsim 6000$ K. This temperature is related only to the phonons directly excited by first order scattering and not to other phonons; otherwise, the SWNT would melt. Thus, during high-bias electron transport, the phonons are not in thermal equilibrium.

TABLE II. Scattering lengths (in nanometers) for the processes in the first column. *Phonon occupation is assumed thermalized at room temperature.* All lengths are in nanometers. In parenthesis are results from direct DFT calculations on $(6, 6)$ and $(11, 11)$ SWNTs with diameter $d = 0.8$ and 1.49 nm, respectively. The other values are obtained by folding the graphene EPCs.

	$d = 0.8$	$d = 1.49$	$d = 2.5$
$l_\mathbf{K}^{bs}$	74 (78)	137 (141)	230
$l_{\Gamma\,TO}^{fs}$	183 (189)	336 (331)	564
$l_{\Gamma\,LO}^{bs}$	183 (215)	336 (362)	564
l_{op}	53	97	163

TABLE I. $|\tilde{D}|^2$ between π states around $\mathbf{K}$.

Backscattering			Forward scattering		
Γ LO	Γ TO	$\mathbf{K}$	Γ LO	Γ TO	$\mathbf{K}$
$2\langle \tilde{D}_\Gamma^2 \rangle_F$	0	$2\langle \tilde{D}_\mathbf{K}^2 \rangle_F$	0	$2\langle \tilde{D}_\Gamma^2 \rangle_F$	0

These results are consistent with the observation that high-bias saturation currents in SWNTs on a substrate are significantly higher than those in suspended SWNTs [28]. Indeed, the effective temperature of optical phonons in suspended SWNTs is expected to be higher due to the absence of a thermally conductive substrate for heat sinking. Also, it was recently reported that electrons inelastically tunneling from a scanning tunneling electron microscope tip into a SWNT induce a nonequilibrium occupation of the radial breathing mode phonons [29]. In this case, the tunneling electrons are mostly coupled with the radial breathing mode, since the associated vibrations directly modulate the tip-nanotube distance. On the contrary, in high-field transport experiments, electrons excite mostly optical phonons, which are the dominant scattering source.

The generation of hot optical phonons, during high-field electron transport, can be directly detected by a Raman scattering experiment combined with electron transport. The occupation of a given phonon mode can be determined from the ratio of the corresponding Stokes and anti-Stokes peak intensities. A rise in this ratio would be direct evidence and would allow one to quantify the hot phonon generation.

Finally, our approach can be easily extended to calculate scattering times and mobility in semiconducting SWNTs. In this case, the scattering times depend on electron energy and chirality since the bands are hyperbolic and the electron density of states is energy dependent. The angles θ, θ', and θ'', entering in Eqs. (6) and (7), are not equal to 0 or π, as in metallic SWNTs, but depend on the chirality and on the initial and final state momenta ($\mathbf{k}$ and $\mathbf{k} + \mathbf{q}$). These angles can be computed by simple geometrical considerations.

In conclusion, accurate DFT calculations of EPCs in graphene, $(6, 6)$ and $(11, 11)$ SWNTs, combined with a simple zone-folding model and the experimental graphite EPCs are used to interpret the saturation SWNTs *I-V* curves of Refs. [4–6]. We show that the optical-phonon occupation is greatly increased during high-bias electron transport, with an effective temperature of thousands Kelvin. Such a high temperature causes a strong reduction of the ballistic scattering length. This suggests coupling the optical-phonon mode with a heat sink in order to reduce their effective temperature. This would increase the scattering length up to the maximum value of Eq. (9), which sets the ultimate limit of ballistic transport. Finally, the phonon generation by electron scattering is analogous to the photon generation by stimulated emission in semiconducting lasers. This suggests that SWNTs, under high bias, can act as a possible source of coherent phonons.

[1] C. T. White and T. N. Todorov, Nature (London) **393**, 240 (1998).

[2] A. Javey, J. Guo, Q. Wang, M. Lundstrom, and H. Dai, Nature (London) **424**, 654 (2003).

[3] S. J. Tans, A. R. M. Verschueren, and C. Dekker, Nature (London) **386**, 474 (1997).

[4] Z. Yao, C. L. Kane, and C. Dekker, Phys. Rev. Lett. **84**, 2941 (2000).

[5] A. Javey *et al.*, Phys. Rev. Lett. **92**, 106804 (2004).

[6] J.-Y. Park *et al.*, Nano Lett. **4**, 517 (2004).

[7] A. Javey, P. Qi, Q. Wang, and H. Dai, Proc. Natl. Acad. Sci. U.S.A. **101**, 13 408 (2004).

[8] R. V. Seidel *et al.*, Nano Lett. **5**, 147 (2005).

[9] J. Jiang, R. Saito, A. Grüneis, G. Dresselhaus, and M. S. Dresselhaus, Chem. Phys. Lett. **392**, 383 (2004).

[10] G. D. Mahan, Phys. Rev. B **68**, 125409 (2003).

[11] G. Pennington and N. Goldsman, Phys. Rev. B **68**, 045426 (2003).

[12] V. Perebeinos, J. Tersoff, and P. Avouris, Phys. Rev. Lett. **94**, 086802 (2005).

[13] J. Jiang *et al.*, Phys. Rev. B **71**, 045417 (2005).

[14] In a first-neighbors TB $|D_\Gamma^{max}|^2 = \eta^2 3/2$, where η is the derivative of the hopping integral with respect to the C-C distance. We compute $|D_\Gamma^{max}|^2$ from the η values reported in the mentioned references. According to our DFT calculations, $|D_\Gamma^{max}|^2 = 91.2$ (eV/Å)^2, corresponding to $\eta = 7.8$ eV/Å.

[15] S. Piscanec, M. Lazzeri, F. Mauri, A. C. Ferrari, and J. Robertson, Phys. Rev. Lett. **93**, 185503 (2004).

[16] R. Saito *et al.*, Appl. Phys. Lett. **60**, 2204 (1992).

[17] V. Zólyomi and J. Kürti, Phys. Rev. B **70**, 085403 (2004).

[18] O. Dubay and G. Kresse, Phys. Rev. B **67**, 035401 (2003).

[19] S. Piscanec *et al.* (unpublished).

[20] We assume that SWNTs at high-bias and low-resistance contacts can be described by the Fermi-liquid theory, as shown in Ref. [4]. The use of Boltzmann theory in Refs. [4–6] requires the same assumption. Luttinger-liquid behavior has been proposed to enhance the scattering with acoustic phonons in the linear response regime: G. Seelig, K. A. Matveev, and A. V. Andreev, Phys. Rev. Lett. **94**, 066802 (2005). This could be relevant in the low-bias regime, where Luttinger-liquid behavior has been observed [4].

[21] C. Thomsen and S. Reich, Phys. Rev. Lett. **85**, 5214 (2000).

[22] R. Saito *et al.*, Phys. Rev. Lett. **88**, 027401 (2002).

[23] The angular dependence of Eqs. (6) and (7) is due to the phase of the electron wave functions. It is derived by TB and reproduces accurately our DFT calculations [15].

[24] J. P. Perdew, K. Burke, and M. Ernzerhof, Phys. Rev. Lett. **77**, 3865 (1996).

[25] N. Troullier and J. L. Martins, Phys. Rev. B **43**, 1993 (1991).

[26] M. Methfessel and A. T. Paxton, Phys. Rev. B **40**, 3616 (1989).

[27] S. Baroni, S. de Gironcoli, A. Dal Corso, and P. Giannozzi, Rev. Mod. Phys. **73**, 515 (2001).

[28] J. Cao, Q. Wang, D. Wang, and H. Dai, Small **1**, 138 (2005).

[29] B. J. LeRoy, S. G. Lemay, J. Kong, and C. Dekker, Nature (London) **432**, 371 (2004).